

Enhanced $0_{g.s.}^+ \rightarrow 2_1^+$ $E2$ transition strength in ^{112}Sn

R. Kumar,^{1,*} P. Doornenbal,² A. Jhingan,¹ R. K. Bhowmik,¹ S. Muralithar,¹ S. Appannababu,³ R. Garg,⁴ J. Gerl,⁵ M. Górska,⁵ J. Kaur,⁶ I. Kojouharov,⁵ S. Mandal,⁴ S. Mukherjee,³ D. Siwal,⁴ A. Sharma,⁷ Pushpendra P. Singh,⁸ R. P. Singh,¹ and H.-J. Wollersheim⁵

¹Inter-University Accelerator Centre, New Delhi 110067, India

²RIKEN Nishina Center for Accelerator-Based Science, Wako, Saitama 351-0198, Japan

³Department of Physics, M.S. University of Baroda, Vadodara 390002, India

⁴Department of Physics & Astrophysics, University of Delhi, Delhi 110007, India

⁵Helmholtzzentrum für Schwerionenforschung GmbH, D-64291 Darmstadt, Germany

⁶Department of Physics, Panjab University, Chandigarh 160014, India

⁷Department of Physics, Bareilly College, Bareilly 243005, India

⁸INFN-Laboratori Nazionali di Legnaro (LNL), I-35020 Legnaro (PD), Italy

(Received 11 September 2009; published 8 February 2010)

Two consecutive Coulomb excitation experiments were performed to excite the 2_1^+ states of $^{112,116}\text{Sn}$ using a ^{58}Ni beam. For ^{112}Sn a $B(E2\uparrow)$ value of $0.242(8) e^2 b^2$ has been determined relative to the known value of ^{116}Sn . The present value is more precise than previous measurements and shows a clear discrepancy from the expected parabolic dependence between the doubly magic nuclei ^{100}Sn and ^{132}Sn . It implies that the reduced transition probabilities are not symmetric with respect to the midshell mass $A = 116$.

DOI: 10.1103/PhysRevC.81.024306

PACS number(s): 23.20.Js, 21.10.Re, 25.70.De, 27.60.+j

I. INTRODUCTION

Numerous experimental and theoretical studies are currently focused on nuclear shell structure far from the line of stability (Ref. [1] and references therein). In particular, the evolution of nuclear properties, for example, the reduced transition probabilities across the $Z = 50$ chain of tin isotopes, has been examined in detail. This constitutes the longest shell-to-shell chain of semimagic nuclei investigated in nuclear structure to date. Radioactive ion beams yield new experimental results close to the doubly magic ^{100}Sn and ^{132}Sn , but very accurate data on the stable midshell nuclei are also of great relevance for our understanding of nuclear structure.

A simple shell model approach to investigating the characteristics of Sn isotopes is to consider ^{100}Sn as an inert core and to treat only neutron degrees of freedom, using the single-particle orbits of the $N = 50$ –82 shell as model space, that is, the five orbits $1g_{7/2}$, $2d_{5/2}$, $2d_{3/2}$, $3s_{1/2}$, and $1h_{11/2}$. Extensive shell model calculations have been performed using this approach [2]. Figure 1 shows the partial level schemes of even- A Sn isotopes with the dominating 6^+ and 10^+ yrast isomers resulting from the filling of the $g_{7/2}$ and $h_{11/2}$ neutron subshells in $A = 102$ –114 and $A = 116$ –130, respectively. These two regions seem to be divided by a soft closed subshell at $N = 64$. If spectroscopic properties of nuclei with more than six or eight valence neutrons are studied with the shell model, the required model space is, however, already exceedingly large. It is therefore appropriate to resort to further simplifications.

In semimagic nuclei, such as Sn isotopes, the seniority scheme provides a very valuable tool for describing low-energy spectra. The nearly constant energy of the first excited 2_1^+ state between $N = 52$ and $N = 80$ [3] is one of the well-

known features of Sn isotopes and is well explained within the generalized seniority model [4]. This seems to indicate that only one of the two kinds of nucleons contributes to the low-energy states. As a consequence, only the isovector ($T = 1$) interaction plays a leading role outside the doubly magic core, which cannot generate quadrupole deformation [5]. Furthermore, according to this theory, the electromagnetic transition rates between the 0^+ ground and the first excited 2_1^+ state exhibit parabolic behavior as a function of mass number across the Sn isotope chain. Thus, for a seniority changing transition, the $B(E2\uparrow)$ values increase at first, peak at midshell ($A = 116$), and fall off thereafter.

The experimental $B(E2; 0_{g.s.}^+ \rightarrow 2_1^+)$ values, henceforth $B(E2\uparrow)$, on the neutron-rich side of the Sn chain follow the theoretical predictions, as can be seen in Fig. 4. For the mass range $A = 116$ –130, the first excited 2_1^+ (seniority $\nu = 2$) state is generally an admixture of different neutron configurations, in contrast to the pure neutron $(h_{11/2})^n$ configuration for the long-lived 10^+ isomeric state. For lighter Sn isotopes, where the neutrons are filling the almost-degenerate single-particle $1g_{7/2}$ and $2d_{5/2}$ states, one observes an unexpected asymmetry in $E2$ strengths with respect to the heavier isotopes. This might indicate that the effective charge values depend on the orbit occupied by the nucleon. Two stable tin isotopes, ^{112}Sn and ^{114}Sn , yield higher $B(E2\uparrow)$ values than expected from shell model calculations, but so far large experimental errors have prohibited further theoretical interpretations. One should also note that the $B(E2\uparrow)$ value obtained for the unstable ^{108}Sn [6] in a Stopped Rare Isotope Spectroscopic INvestigation at GSI (RISING) experiment is based on a measurement relative to ^{112}Sn .

II. MOTIVATION AND EXPERIMENTAL DETAILS

The large uncertainty in the $B(E2\uparrow)$ values in ^{112}Sn and ^{114}Sn motivated two Coulomb excitation experiments to

*rakuiuc@gmail.com

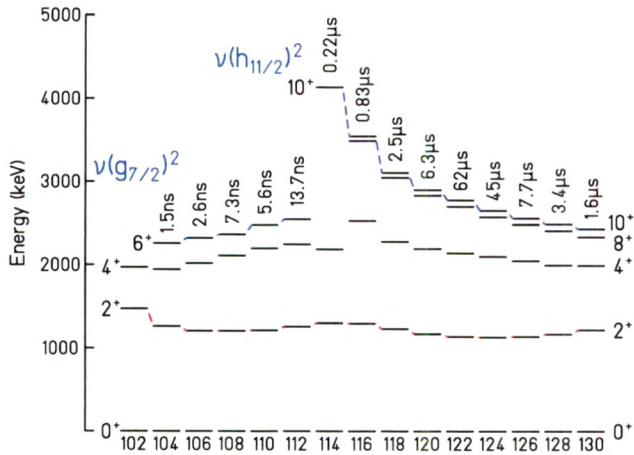


FIG. 1. (Color online) Partial level schemes [12] and isomer systematics in even- A Sn nuclei for mass numbers between $A = 102$ and $A = 130$. Levels of the same spin and positive parity are connected by dashed lines.

improve these crucial data points. In a previous measurement, the $B(E2\uparrow)$ value of ^{114}Sn was determined at the GSI (Helmholtzzentrum für Schwerionenforschung GmbH) [7]. The result showed an unexpected enhancement relative to the $B(E2\uparrow)$ of ^{116}Sn . This paper reports the results of a Coulomb excitation experiment and the measurement of the corresponding $B(E2\uparrow)$ value for ^{112}Sn . The literature value [3] for ^{112}Sn is mainly based on two rather accurate measurements [8,9], which differ by more than 11%. As there is no explanation given for the discrepancy [9], a detailed study of the reduced transition probabilities for the tin isotopes requires an additional measurement. The present experiment was performed at the Inter-University Accelerator Centre (IUAC) in New Delhi. Two targets, ~ 0.53 mg/cm 2 ^{112}Sn (99.5% enriched) and ^{116}Sn (98% enriched), were bombarded with ^{58}Ni ions at an incident energy of 175 MeV, which is well below the Coulomb barrier, to ensure pure electromagnetic interaction. In two consecutive experiments the relative excitation strength of the 2^+ state in ^{112}Sn and ^{116}Sn was determined, with the first excited 2^+ state in ^{58}Ni used for normalization. This ensured that systematic errors were excluded and the projectile excitation canceled in the $^{112}\text{Sn}/^{116}\text{Sn}$ γ -ray yield ratio. The γ -ray ratio is a direct measure of the $B(E2\uparrow)$ of ^{112}Sn relative to that of ^{116}Sn . Because the adopted $B(E2\uparrow)$ value for ^{116}Sn , $0.209(6)$ e 2 b 2 , is an evaluation of 11 different experimental results [3], it becomes a reliable and precise reference point.

Scattered projectiles and recoils were detected in an annular gas-filled parallel-plate avalanche counter (PPAC), subtending the angular range $15^\circ \leq \vartheta_{\text{lab}} \leq 45^\circ$ in the forward direction. This detector was placed 11 cm from the target and was position sensitive in both the azimuthal and the polar angles. The azimuthal angle φ was obtained from the anode foil, which was divided into 20 radial sections of 18° each. To measure the polar angle ϑ , the cathode was patterned in concentric conductor rings, each 1 mm wide, with an insulating gap of 0.5 mm between them. Each ring was connected to its neighbor by a delay line of 2 ns. The cathode signals were read out from

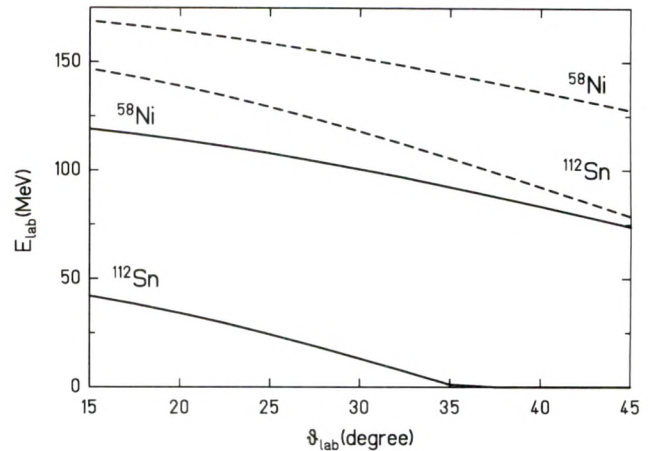


FIG. 2. Kinetic energies of scattered ^{58}Ni projectiles and ^{112}Sn recoils detected in the angular range of 15° to 45° covered by the PPAC. Dashed lines are based on two-body kinematics for a beam energy of 175 MeV, whereas solid lines are corrected for energy loss [10] in a $10\text{-}\mu\text{m}$ Mylar foil, which was used as the entrance window of the PPAC.

the innermost and outermost rings, and the ϑ information was derived from the time difference between the anode and the cathode signals. For technical reasons, only 14 of the anode segments were used in the experiment. An entrance window of $10\text{-}\mu\text{m}$ -thick Mylar was used for the PPAC, which reduced the kinetic energy of both reaction partners. Whereas ^{58}Ni projectiles could still be measured in the PPAC, Sn recoils either were stopped in the entrance window or were close to the detection limit. Figure 2 shows qualitatively the effect of $10\text{-}\mu\text{m}$ -thick Mylar foil on the kinetic energy of both reaction partners. In this way distant collisions (Ni detected in PPAC) could be distinguished from close collisions (Sn detected).

De-excitation γ -rays were detected in four clover detectors mounted at $\vartheta_\gamma \sim 135^\circ$ with respect to the beam direction at a distance of ~ 22 cm to the target. The φ_γ angles for the clover detectors were $\pm 55^\circ$ and $\pm 125^\circ$ with respect to the vertical direction. Individual energies of the 16-Ge crystals and common timing signals of the four clover detectors were recorded in coincidence with the PPAC anode and cathode signals event by event. Low-energy radiations were suppressed using Cu, Sn, and Pb absorbers of thicknesses between 0.5 and 0.7 mm placed in front of the clover detectors. To avoid any systematic error, the ^{112}Sn and ^{116}Sn targets were used in turn every 3 h, for a total measuring time of approximately 50 h. Energy and relative efficiency calibrations were carried out using a ^{152}Eu source.

III. DATA ANALYSIS AND RESULT

The particle identification and the particle position measurement allowed for a precise Doppler correction of the measured γ -ray energies. From the measured (ϑ, φ) angle of the scattered Ni projectiles, the velocities of both reaction partners and the recoil angles could be calculated from two-particle kinematics. In the analysis, an add-back procedure (applied to

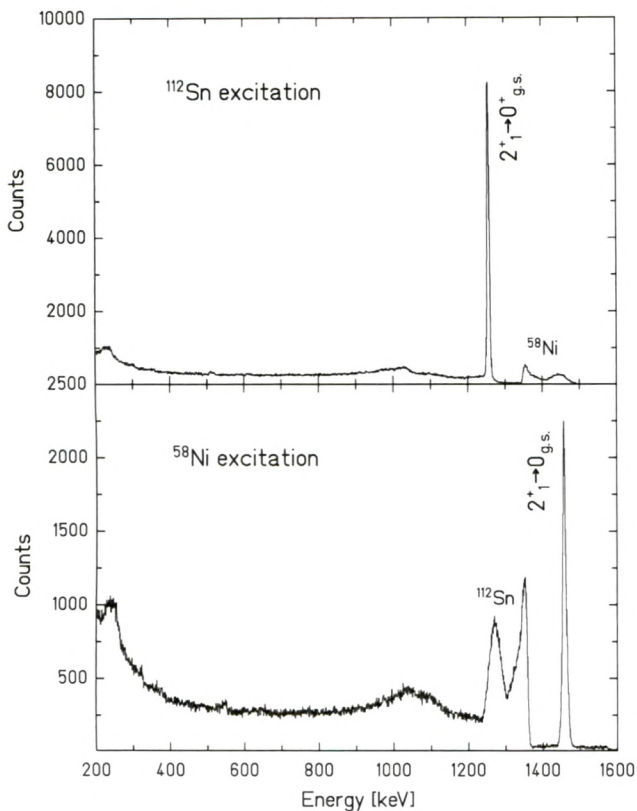


FIG. 3. Doppler-corrected γ -ray spectra emitted from ^{112}Sn target nuclei (top) and ^{58}Ni projectiles (bottom) in the reaction $^{112}\text{Sn}(^{58}\text{Ni}, ^{58}\text{Ni}^*)^{112}\text{Sn}$ at 175 MeV. Scattered ^{58}Ni projectiles were detected in the PPAC and clover detectors were operated in the add-back mode.

all four crystals within each Ge clover) and a Doppler shift correction were performed for each clover detector ($\vartheta_\gamma, \varphi_\gamma$) event by event. Figure 3 shows the Doppler-corrected spectra for ^{112}Sn excitation (top) and ^{58}Ni excitation (bottom) with the dominating $2_1^+ \rightarrow 0_{g.s.}^+$ transitions. Higher excited states were not observed. A γ -ray resolution of 13 keV (full width at half-maximum; FWHM) was obtained for target excitation, and 7 keV (FWHM) for projectile excitation, which results from the finite solid angle of the γ -ray detector (intrinsic resolution, <3 keV).

From observation of the Doppler-corrected γ -ray lines corresponding to $2_1^+ \rightarrow 0_{g.s.}^+$ transitions, the target and projectile excitation can be extracted. The $B(E2\uparrow)$ value of ^{112}Sn was obtained from the experimental γ -ray intensity double ratio $[I_\gamma(^{112}\text{Sn})/I_\gamma(^{58}\text{Ni})]/[I_\gamma(^{116}\text{Sn})/I_\gamma(^{58}\text{Ni})]$ of the $2_1^+ \rightarrow 0_{g.s.}^+$ decays. This double ratio was corrected for the different Ge detector efficiency (1.7%) and target enrichments (1.5%). Coulomb excitation calculations were performed with the Winther-de Boer Coulex code [11]. Calculations included the feeding contributions from the $0_2^+, 2_2^+, 3_1^-,$ and 4_1^+ states in ^{112}Sn and ^{116}Sn , which were obtained from the known excitation strengths given in Ref. [12]. In both cases the summed intensity from decays of higher-lying states added up to less than 2% of the $2_1^+ \rightarrow 0_{g.s.}^+$ decay intensity, which

agreed with our experimental findings. The calculated double ratio changed by less than 1% when the feeding states were neglected. The slowing-down of the projectiles in the targets (0.8%), the uncertainty of the PPAC boundaries (0.5%), and the adopted ^{116}Sn $B(E2\uparrow)$ value (3%) were also considered. In the second step, the γ -ray decay was calculated taking into account the particle- γ angular correlation (0.8%), the internal conversion, and the finite geometry of the γ detector. The $0_{g.s.}^+ \rightarrow 2_1^+$ matrix element in ^{112}Sn was adjusted in the Coulex calculations to reproduce the experimental double ratio. The resulting $B(E2\uparrow)$ value in ^{112}Sn is $0.242(8) e^2 b^2$. It is consistent with previous values [3,13,14] but has a higher precision. The error is the quadratic sum of the four individual uncertainties mentioned previously and the uncertainty of the γ -ray intensities (1%). Because the largest contribution to the error of ^{112}Sn and ^{114}Sn [7] results from the uncertainty of the $B(E2\uparrow)$ value in ^{116}Sn , the mass dependence was determined with an even higher accuracy. Moreover, the new result will influence the RISING data for ^{108}Sn that were deduced relative to the adopted value for ^{112}Sn . A renormalization using our new $B(E2\uparrow)$ value for ^{112}Sn leads to a value of $B(E2\uparrow) = 0.232(57) e^2 b^2$ for ^{108}Sn .

IV. DISCUSSION

The experimental information in the $B(E2\uparrow)$ systematics on tin isotopes with the new value of ^{112}Sn included is presented in Fig. 4 and listed in Table I. It is apparent that the result for ^{112}Sn is about 20% larger than that for ^{120}Sn , in contrast to the symmetric distribution expected with respect to the midshell $A = 116$. According to the seniority model the $B(E2\uparrow)$ values naturally decrease with a decreasing number of particles outside the closed core. This trend cannot be found in our data for ^{112}Sn and ^{114}Sn [7]. As the experimental $B(E2\uparrow)$ value already increases when

TABLE I. Comparison of measured $B(E2\uparrow)$ values for Sn isotopes with calculated data [18]. Experimental data on neutron-deficient isotopes are averaged values from Refs. [6] and [15–17].

Isotope	$E_{2_1^+}$ (keV)		$B(E2\uparrow) e^2 b^2$	
	Exp	RQRPA	Exp	RQRPA
^{102}Sn	1472.0(2)	1341		0.094
^{104}Sn	1260.1(3)	1001		0.185
^{106}Sn	1207.7(5)	891	0.209(32)	0.235
^{108}Sn	1206.1(2)	940	0.224(16)	0.227
^{110}Sn	1211.9(2)	1014	0.226(18)	0.202
^{112}Sn	1256.9(7)	1112	0.242(8)	0.176
^{114}Sn	1299.9(7)	1207	0.232(8)	0.155
^{116}Sn	1293.6(8)	1236	0.209(6)	0.144
^{118}Sn	1229.7(2)	1242	0.209(8)	0.146
^{120}Sn	1171.3(2)	1269	0.202(4)	0.150
^{122}Sn	1140.6(3)	1296	0.192(4)	0.152
^{124}Sn	1131.7(2)	1340	0.166(4)	0.145
^{126}Sn	1141.2(2)	1411	0.10(3)	0.126
^{128}Sn	1168.8(4)	1537	0.073(6)	0.096
^{130}Sn	1121.3(5)	1751	0.023(5)	0.055

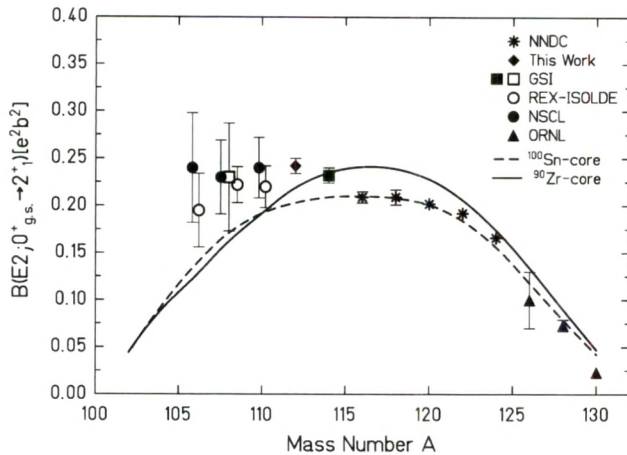


FIG. 4. Experimental data on $B(E2; 0_{g.s.}^+ \rightarrow 2_1^+)$ values in the Sn isotope chain from the current result for ^{112}Sn and from Refs. [3,6,7], and [15–17]. Dashed and solid lines show the predictions of the large-scale shell model calculations from Ref. [6] performed with a ^{100}Sn core and a ^{90}Zr core, respectively.

going from ^{116}Sn to ^{114}Sn , it appears that proton excitations play an important role in the transition. Banu *et al.* [6] include up to 4p-4h proton core excitations in their calculations by means of a seniority truncated model space outside of a ^{90}Zr core. Because of the seniority truncation in that calculation the systematic trend in $B(E2\uparrow)$ values was retained. The comparison between experiment and theory shows agreement for the heavier Sn isotopes assuming a ^{100}Sn core. However, for the lighter Sn isotopes asymmetry of the $B(E2\uparrow)$ systematics is observed. This indicates a different character of the core excitations in the $N = Z$ and $N > Z$ regions of the tin isotopic chain.

With reference to Fig. 1, as already pointed out, there seems to be a subshell closure at $N = 64$ for the Sn isotope chain. Below this boundary, the level structure is dominated by the $(d_{5/2})^2$ and $(g_{7/2})^2$ components, whereas the $(h_{11/2})^2$ component governs the heavier Sn decay schemes. Around $N = 64$, all single-particle configurations contribute approximately equally and yield an increased excitation energy of

the 2_1^+ states in ^{114}Sn and ^{116}Sn compared with the other Sn isotopes. However, reduced transition probabilities test nuclear structure in still greater detail than excitation energies, because the former involve the wave functions of the initial and final states.

Recently [18], the relativistic quasiparticle random-phase approximation (RQRPA) has been applied to calculate the energies of the first excited 2^+ states and corresponding $B(E2\uparrow)$ values for tin isotopes with even mass numbers $A = 100$ –134. The great advantage of this RQRPA scheme is that it is not necessary to assume an inert core and to adjust parameters of the Hamiltonian from nucleus to nucleus or region to region of the periodic table. In Table I we compare the measured $B(E2\uparrow)$ values of the Sn isotopes with the calculated data [18]. Considering that there is no free adjustment of parameters or effective charges, the agreement with the theoretical data is very good. The most important feature is the asymmetric behavior of the $B(E2\uparrow)$ data with respect to the midshell nucleus ^{116}Sn . It is interesting to note that the same RQRPA calculations yield quite satisfactory agreement also for the Ni and Pb isotopes [19].

In conclusion, the $B(E2; 0_{g.s.}^+ \rightarrow 2_1^+)$ value in stable ^{112}Sn was measured relative to the well-known result for ^{116}Sn in a Coulomb excitation experiment. The observation from the experimental $B(E2\uparrow)$ value increases upon going from ^{116}Sn to ^{112}Sn , which indicates that the generalized seniority scheme fails to describe the $B(E2\uparrow)$ systematics for Sn isotopes. The experimental data are also compared with RQRPA calculations that predict the observed asymmetric behavior of the $B(E2\uparrow)$ values with respect to the midshell nucleus with $N = 66$.

ACKNOWLEDGMENTS

The authors would like to thank N. Madhavan for many helpful discussions and S. K. Saini, A. Kotari, and R. Ahuja for their significant contribution to the experiment. Thanks go to the operating staff of the Inter-University Accelerator Centre (IUAC) accelerator for supplying the excellent Ni beam. This work was performed under IUAC-GSI collaboration. P.D. acknowledges the financial support given by the Japan Society for the Promotion of Science.

- [1] H. Grawe and M. Lewitowicz, Nucl. Phys. **A693**, 116 (2001).
- [2] M. Hjorth-Jensen, T. T. S. Kuo, and E. Osnes, Phys. Rep. **261**, 125 (1995).
- [3] S. Raman, C. W. Nestor, and P. Tikkanen, At. Data Nucl. Data Tables **78**, 1 (2001).
- [4] I. Talmi, Nucl. Phys. **A172**, 1 (1971).
- [5] R. Casten, *Nuclear Structure from a Simple Perspective* (Oxford University Press, New York, 2000).
- [6] A. Banu *et al.*, Phys. Rev. C **72**, 061305(R) (2005).
- [7] P. Doornenbal *et al.*, Phys. Rev. C **78**, 031303(R) (2008).
- [8] P. H. Stelson *et al.*, Phys. Rev. C **2**, 2015 (1970).
- [9] R. Graetzer *et al.*, Phys. Rev. C **12**, 1462 (1975).
- [10] L. C. Northcliffe and R. F. Schilling, Nucl. Data Tables A **7**, 233 (1970).
- [11] A. Winther and J. de Boer, in *Coulomb Excitation*, edited by K. Alder and A. Winther (Academic Press, New York, 1966).
- [12] <http://www.nndc.bnl.gov/ensdf/>.
- [13] J. N. Orce *et al.*, Phys. Rev. C **76**, 021302(R) (2007).
- [14] J. N. Orce *et al.*, Phys. Rev. C **77**, 029902(E) (2008).
- [15] D. C. Radford *et al.*, Nucl. Phys. **A752**, 264c (2005).
- [16] J. Cederkäll *et al.*, Phys. Rev. Lett. **98**, 172501 (2007).
- [17] A. Ekström *et al.*, Phys. Rev. Lett. **101**, 012502 (2008).
- [18] A. Ansari, Phys. Lett. **B623**, 37 (2005).
- [19] A. Ansari and P. Ring, Phys. Rev. C **74**, 054313 (2006).



Contents lists available at ScienceDirect

Nuclear Instruments and Methods in Physics Research A

journal homepage: www.elsevier.com/locate/nima

Testing of a DSSSD detector for the stopped RISING project

R. Kumar^{a,b,*}, F.G. Molina^c, S. Pietri^d, E. Casarejos^f, A. Algora^{c,g}, J. Benlliure^f, P. Doornenbal^{e,b}, J. Gerl^b, M. Gorska^b, I. Kojouharov^b, Zs. Podolyák^d, W. Prokopowicz^b, P.H. Regan^d, B. Rubio^c, H. Schaffner^b, S. Tashenov^b, H.-J. Wollersheim^b

^a Inter University Accelerator Centre, New Delhi 110067, India

^b Gesellschaft für Schwerionenforschung (GSI), D-64291 Darmstadt, Germany

^c Instituto de Física Corpuscular, CSIC-Univ. Valencia, E 46071 Valencia, Spain

^d Department of Physics, University of Surrey, Guildford GU2 7XH, UK

^e Institut für Kernphysik, Universität zu Köln, D-50937 Köln, Germany

^f Departamento de Física de partículas, Universidad de Santiago de Compostela, E-15782 Santiago de Compostela, Spain

^g Institute of Nuclear Research of the Hungarian Academy of Sciences, POB 51, 4001 Debrecen, Hungary

ARTICLE INFO

Article history:

Received 3 June 2008

Received in revised form

18 August 2008

Accepted 20 August 2008

Available online 1 November 2008

Keywords:

β -decay

HI implantation

Silicon detectors

ABSTRACT

An active stopper for the RISING project at GSI has been developed for β -decay studies and conversion electron spectroscopy following projectile fragmentation/fission reactions. This system employs six double-sided silicon strip detectors in the final focal plane of the GSI FRagment Separator (FRS) to detect both the fragment implantations and their subsequent charged-particle (α , β , p) decays. The wide range of energy response required (150 keV up to several GeVs) was covered by the use of a logarithmic preamplifier. Measurements with a ^{207}Bi conversion electron source yielded an energy resolution of 20 keV at electron energies of ~ 1 MeV and a detection threshold of 150 keV. The response to the implantation of 400 AMeV ^{136}Xe ions in the active stopper is also discussed in the present paper.

© 2008 Elsevier B.V. All rights reserved.

1. Introduction

A new beta counting system has been developed for the RISING (Rare Isotope Spectroscopic INvestigation at GSI) project [1] to study the β -decay of exotic nuclei produced by projectile fragmentation and in-flight fission. The system employs up to six Micron Semiconductor Ltd. [2] Model W1(DS)-1000 DC coupled double-sided silicon strip detectors (DSSSD) with thickness of 1 mm to detect both fragment implantations and their subsequent β -decays. While this detector thickness provides an efficient implantation of heavy ions, the range of the β -particles emitted by the nuclear decays is usually significantly larger than 1 mm of silicon. This fact results in the probable escape of the particles from the DSSSD before they deposit their full kinetic energy. The deposited energy depends on the path of the electron in the silicon and therefore on the implantation depth. Fig. 1 (left) shows the simulated energy spectrum of the electrons emitted by the β -decay and detected by the DSSSD. A Fermi–Curie initial electron energy distribution with $Q_{\beta} = 5$ MeV was assumed. For different Q_{β} -values the simulated energy distribution only

changes on the high-energetic side. The Monte-Carlo simulations were performed using the GEANT4 simulation toolkit [3] with the 'GEANT4 Low Energy Electromagnetic Physics' package [4]. Two cases of the implantation were considered: uniformly distributed and exact central implantation. In the later case the minimum distance to the surface is 0.5 mm, which corresponds to the minimum energy of 0.1 MeV that the electrons deposit in the crystal. This fact highlights the importance of achieving the low-energy threshold at 0.1 MeV as well as the importance of the accurate central implantation. Fig. 1 (right) shows the efficiency to detect β -particles in the 1 mm thick DSSSD as a function of the low-energy threshold for the two considered implantation scenarios. The efficiency is clearly high for a low detection threshold.

The array of six DSSSDs can be used in different configurations. The most common is to use three detectors positioned in two rows, one behind the other, at the final focal plane of the FRagment Separator (FRS) [5] which is used for the selection and identification of the radioactive nuclei. Each detector consists of 16 front strips and 16 back strips, each of width 3 mm, thus providing $256 \times 3 \times 3 \text{ mm}^2$ pixels on a $5 \times 5 \text{ cm}^2$ detector to encode x - y positions. A variable thickness aluminium degrader is used just in front of the DSSSD array to slow down the ions such that they are implanted in the active stopper at the centre of the stopped RISING germanium array [1]. Implantation and β -decay

*Corresponding author at: Inter University Accelerator Centre, New Delhi 110067, India. Tel.: +91 9868207046.

E-mail address: rakuuiac@gmail.com (R. Kumar).

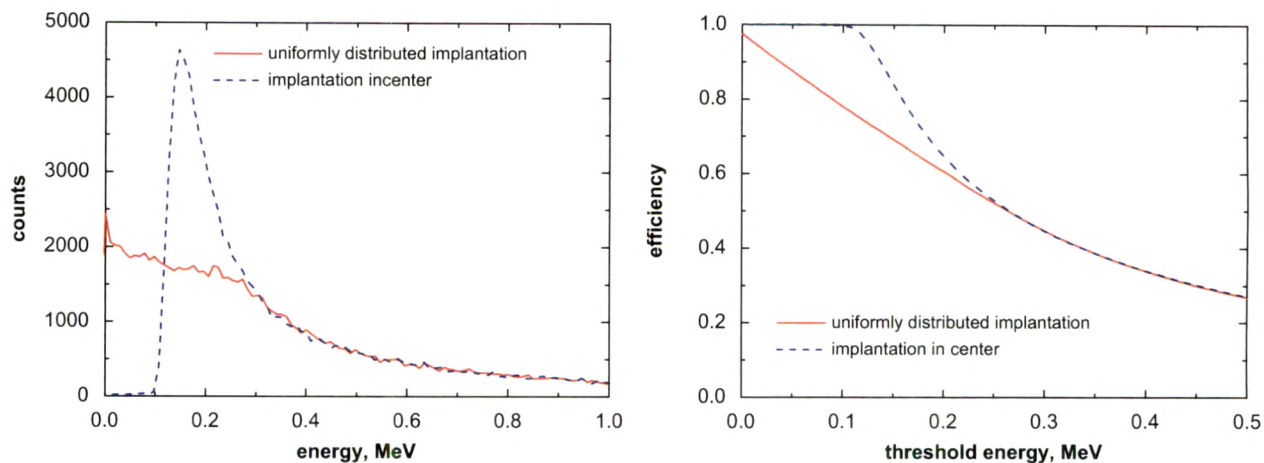


Fig. 1. Simulated energy spectrum of β -particles emitted from fragments implanted uniformly (solid line) and exactly in the centre (dashed line) of a DSSSD (left). The simulation assumes a Q_{β} -value of 5 MeV and a Fermi–Curie distribution for β -particles. The right figure shows the calculated β -detection efficiency as a function of the DSSSD threshold for the two considered implantation scenarios discussed in the text.

events are directly correlated within each pixel of the detector, which requires accurate knowledge of the implantation position. The half-life of the nucleus is deduced from the time correlation between the implantation time of the identified fragments in the active catcher and the subsequent β -decay. The time correlation is measured with a time stamping system providing a resolution of 25 ns.

One of the challenges in designing the electronics for the beta counting system is the range of charged particle energies that must be measured. A fast fragment implantation will deposit more than 1 GeV total energy when it is stopped in the centre of the DSSSD, while an emitted β -particle will deposit less than 1 MeV. Measurements with *Mesytec* [6] electronics are described in Section 2. The experimental results with a ^{207}Bi β -source are compared with the data taken with *Multi Channel Systems* [7] electronics in Section 3. Finally, a measurement with ^{136}Xe ions was performed in order to investigate the heavy-ion implantation response in the DSSSD. These results are presented in Section 4.

2. Measurements with *Mesytec* electronics

The *Mesytec* MPR-32 preamplifier is a 32-channel input preamplifier which was used for the 16 front and 16 back strips of a single DSSSD. It can accept positive or negative input polarities. The *Mesytec* MPR-32 multi-channel preamplifier is available in a linear or logarithmic mode. For the linear MPR-32 preamplifier an amplification range of 5 or 25 MeV can be chosen. For the 978 keV line seen from the ^{207}Bi conversion electron source the MPR-32 output signal has a pulse height of approximately 200 mV and its signal-to-noise ratio is 10:1 (5 MeV range). The logarithmic MPR-32 preamplifier provides a linear range of 2.5 or 10 MeV, which covers 70% of the total range. The last 30% covers the energy range from 10 MeV up to 3 GeV. Both MPR-32 units have a full voltage range of preamplifier output of 4 V. Fig. 2 shows the characteristics of the logarithmic MPR-32 preamplifier which was measured with a research pulser. It is worth mentioning that the pulse height cannot be directly related to the implantation energy because of the pulse height defect in solid state detectors.

The MPR-32 was combined with two *Mesytec* STM-16 shaping-/timing filter/discriminator modules when the differential input version is used. The STM-16 is a NIM-powered device which

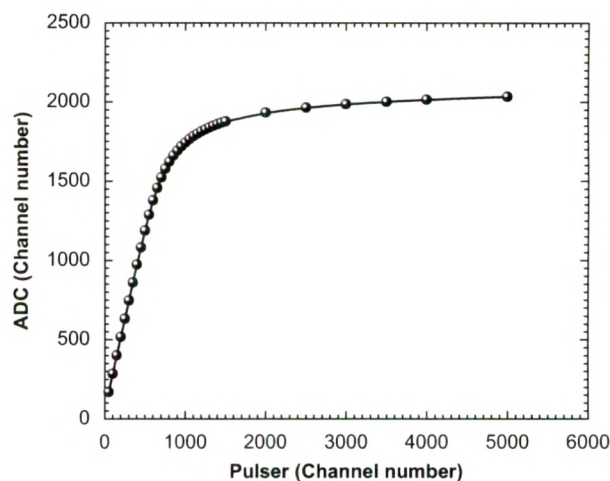


Fig. 2. The characteristics of the logarithmic MPR-32 preamplifier was measured with a 10 MeV linear range setting and STM-16 spectroscopy amplifiers.

has 16 input channels allowing parallel processing. The gain was adjusted individually in 16 steps with a maximum gain of 30. A shaping time of 1 or 2.5 μs (FWHM) was chosen. For the following measurements a shaping time of 1 μs (FWHM) was selected as this would be needed for higher count rate experiments.

The STM-16 was controlled by a NIM-module MRC-1 which works as a bus master. One *Mesytec* MRC-1 can control 32 various *Mesytec* modules (not only STM-16). It is prepared for the remote control of (i) individual discriminator thresholds (0–40% of maximum range, 4 V) and (ii) gains (in 16 steps) for pairs of channels. Communication with a control PC is done via RS-232 serial interface. Each analogue signal was fed directly to a CAEN V785AF VME-ADC which has a maximum input voltage of 8 V. The trigger signal of STM-16 is a logical OR of the 16 discriminator channels and was used to produce the ADC gate. In Fig. 3 semi-logarithmic energy spectra of a ^{207}Bi β -source are shown for different discriminator thresholds of the *Mesytec* STM-16 module. As can be seen, the detection limit for electron measurements using this system was set as low as 150 keV with the present electronics and the detectors/electronics working at room

temperature. This limit was defined at 50% of the logarithmic spectral curvature caused by the discriminator threshold.

3. Energy resolution measured with electrons of a ^{207}Bi source

First, a standard ^{241}Am source was used to verify the performance of the DSSSD and to measure the resolution of the system. The alpha source was placed 5 cm from the detector's surface in a vacuum vessel. Individual strips displayed energy resolutions of 0.48–0.52% (front) and 0.51–0.64% (back) FWHM for the 5.5 MeV peak. Then a ^{207}Bi source, which emits mono-energetic conversion electrons, was used to calibrate the DSSSD. The ^{207}Bi source was covered with $70\ \mu\text{g}/\text{cm}^2$ polypropylene foil and positioned at 5 cm from the front face of the detector. The measured electron peak spectrum for a front strip is shown in Fig. 4 (left). Four peaks (482, 555, 976 and 1049 keV) are clearly

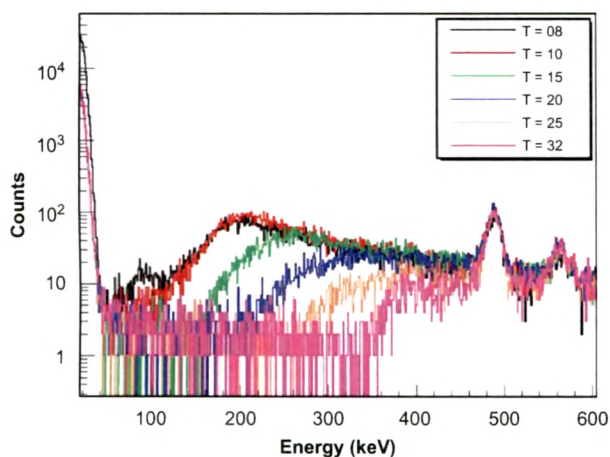


Fig. 3. Energy spectra of a ^{207}Bi β -source measured for different discriminator thresholds labelled $T = 8$ – 32 of the Mesytec STM-16 module.

observed, due to K and L + M + N conversion electrons of the 570 keV (E2) and 1060 keV (M4) transition in ^{207}Pb . The energy resolution of the 976 keV line is 14.4 keV (FWHM) for this strip. Fig. 4 (right) shows an overview of the energy resolution as a function of the strip number. The front junction side of the detector has clearly got better resolution compared to the rear ohmic side. A comparison between the linear and logarithmic MPR-32 preamplifier reveals a slightly poorer energy resolution in the logarithmic one, 19.7 keV compared to 15.3 keV for a selected front strip of the DSSSD-2243-5. However, the logarithmic MPR-32 has the advantage of being able to measure both the heavy-ion implantation as well as the β -particle. All the data discussed so far were obtained for detector tests performed in vacuum. DSSSD tests were also carried out in dry nitrogen. The energy resolutions measured in vacuum and dry nitrogen were the same within the experimental uncertainties. Therefore, the RISING experiments with an active stopper can be performed in dry nitrogen, allowing the use of a detector vessel with thin walls, thereby minimizing the absorption of the emitted γ -rays.

At the National Superconducting Cyclotron Laboratory (NSCL) at Michigan State University (MSU), a beta counting system [8] has been developed with different electronics which yields reliable energy information for both implants and decays. The DSSSD signals are first processed by two 16-channel charge sensitive preamplifier modules CPA-16 supplied by Multi Channel Systems [7]. These modules contain precision pre- and shaping amplifier electronics and provide both high gain (2 V/pC) and low gain (0.1 V/pC) analogue outputs. They have a full voltage range of preamplifier output of 5 V. The high gain signals carry information from low-energy β -decay events, and they require further amplification. This is accomplished at MSU using Pico Systems [9] 16-channel shaper/discriminator modules in CAMAC. The shaper output of the Pico Systems module is sent directly to an ADC. For the present DSSSD tests two 16-channel charge sensitive preamplifier modules CPA-16 were also tested at GSI. For a ^{207}Bi β -source the CPA-16 output signals have a pulse height of approximately 200 mV and a signal-to-noise ratio of 7:1. At GSI ORTEC 572 and 16-channel CAEN N568BC amplifiers were used for

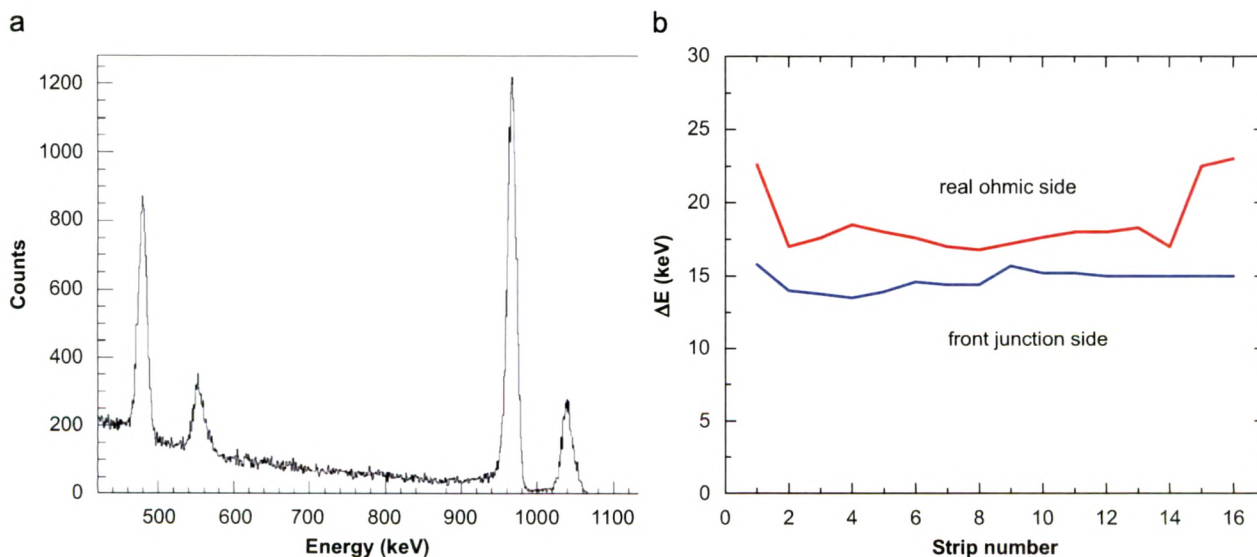


Fig. 4. The conversion electron spectrum of ^{207}Bi measured with a linear MPR-32 preamplifier for a front strip of DSSSD-2512-17. The four peaks at 482, 555, 976 and 1049 keV result from mono-energetic electrons—see text for details (left). The energy resolution for the front junction and the rear ohmic side versus the strip number is plotted on the right side.

shaping the high gain CPA-16 output signals. Three different measurements were performed: (i) the high gain output signal of the CPA-16 preamplifier was sent directly to the CAEN V785AF VME-ADC, (ii) it was additionally amplified using an ORTEC 572 amplifier with shaping times of 0.5, 1.0 and 2.0 μ s, respectively, and (iii) using a CAEN N568BC module with a shaping time 2.0 μ s before sending it to the same ADC. Fig. 5 shows the conversion electron spectrum of ^{207}Bi without further amplification. Only two peaks (482 and 976 keV) were clearly seen in the energy spectrum, due to K conversion electrons of the 570 and 1060 keV transitions in ^{207}Pb . The energy resolution of the 976 keV line varied between 100 and 120 keV depending on the different measurements. The detection limit for electrons was found to be approximately 300 keV.

In summary, with a ^{207}Bi source an energy resolution of 15–20 keV and an energy threshold of 150 keV were obtained for the Mesytec electronic, compared to a FWHM of 100 keV and a threshold of 300 keV for Multi Channel Systems electronics. Since conversion electron spectroscopy studies are also part of the

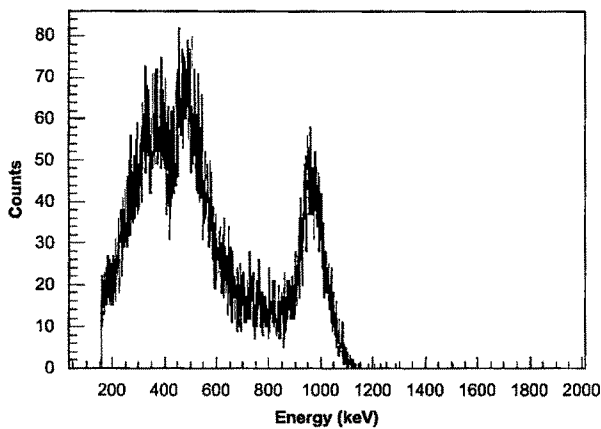


Fig. 5. The conversion electron spectrum of ^{207}Bi measured with the multi-channels electronics for the same strip of DSSSD-2243-5. The two peaks at 482 and 976 keV result from mono-energetic electrons.

RISING stopped beam campaign the Mesytec electronic was selected for the readout of the DSSSDs.

4. Implantation measurement with a ^{136}Xe beam

A test measurement has been performed with the RISING set-up to investigate the heavy-ion implantation in the DSSSD. A primary beam of ^{136}Xe with an initial energy of 400 A MeV was slowed down in the aluminium degrader and implanted in the Si-detector. The active stopper vessel for the DSSSD was made out of Pertinax (phenolic-formaldehyde cellulose-paper PF CP 2061) with an entrance and exit window covered by a thin black Pocalon C foil of thickness 20 μ m. The Pertinax wall was 2 mm thick, corresponding to an aluminium equivalent for γ -transmission of 0.7 mm.

Two measurements, triggered by a scintillation detector for beam particles in the FRS, were carried out with the linear and logarithmic MPR-32 preamplifiers. The linear MPR-32 preamplifier is well suited for the electron measurement (MeV range), however, for the implantation of heavy ions (GeV range) the output signals saturate. The energy spectra (see e.g. Fig. 7) show the low-energetic part of the implantation caused by light charged particles and atomic X-rays. In most cases all the strips of the DSSSD fire (see Fig. 6, left), since no condition is set on the implantation of the heavy ions. If only the overflow data of the energy spectra (>10 MeV) are considered (see Fig. 6, right), the multiplicity spectrum is localized at small values, which is expected for the implantation. For multiplicity one on each side of the DSSSD the position is uniquely determined, while for higher multiplicities the centroid has to be determined. When using the linear MPR-32 preamplifier each saturated strip has the same weight for this calculation, since the individual strip energies above 10 MeV are not measured. Therefore, the overflow data of the DSSSD only allow a zero order position determination of the heavy-ion implantation. Based on the multiplicity distribution (Fig. 6, right) one obtains an average shift of 2.3 mm ($0.75 \times \text{strip width}$) for each event.

The logarithmic MPR-32 preamplifier is well suited for both electron measurement (MeV range) and heavy-ion implantation (GeV range). The measured energy spectrum (10 MeV range

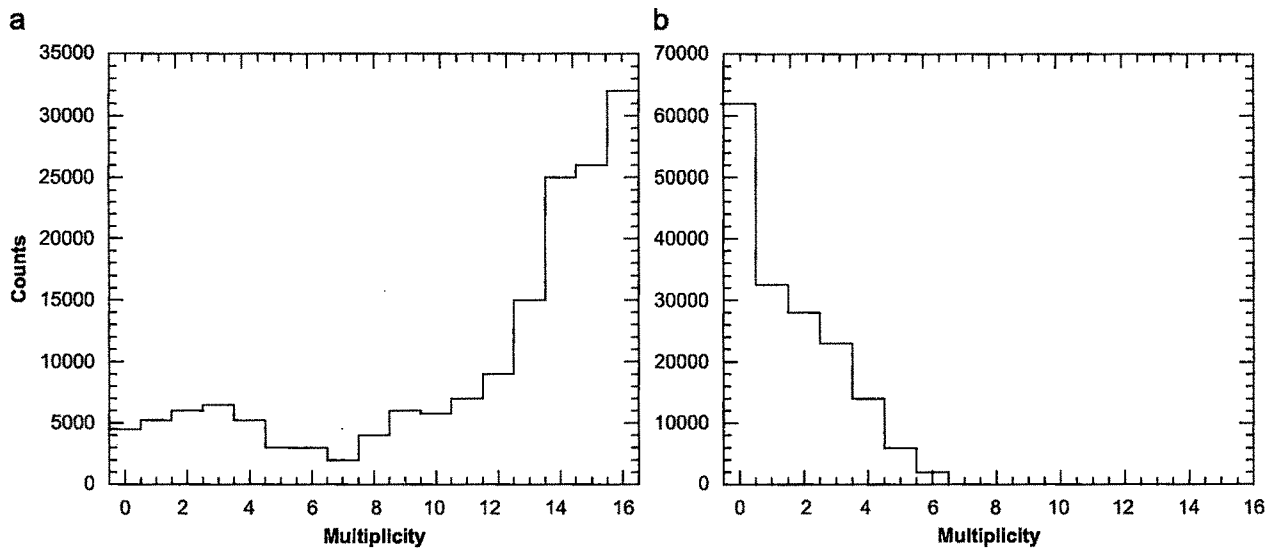


Fig. 6. Multiplicity distributions measured by x-strips for different energy thresholds. For a very low-energy threshold almost all x-strips are firing (left), while for the overflow (>10 MeV) data the hit probability is very low (right), as expected for the implantation of ^{136}Xe ions.

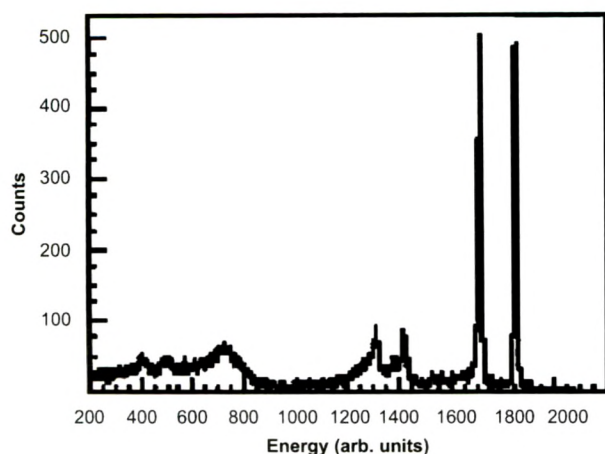


Fig. 7. Measured energy spectrum (10MeV range for the linear part of the logarithmic MPR-32 preamplifier) obtained by a x-strip (front junction) for the implantation of ^{136}Xe ions. The double hump structure around 1600 and 1800 is related to the stopping of the heavy ions.

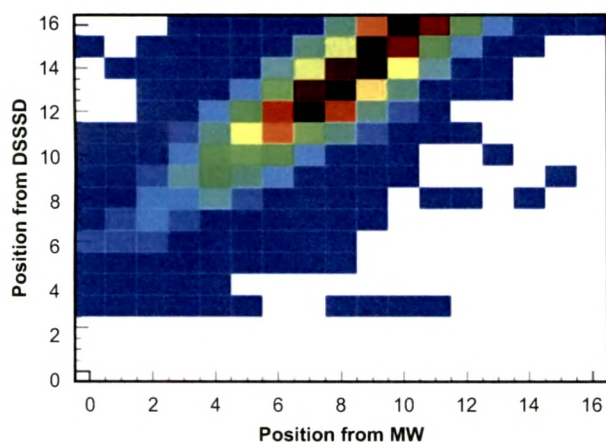


Fig. 8. Position correlation in x direction between the DSSSD and the multi-wire (MW) detector of the FRS. For the DSSSD the position of the implanted ^{136}Xe ion was determined from the mean of highest energy peaks, when a logarithmic MPR-32 preamplifier was used. The position of the MW was projected on the strip number of the DSSSD.

setting for the linear part of the logarithmic preamplifier) obtained from a x-strip (front junction) is shown in Fig. 7 for the implantation of ^{136}Xe ions. It shows a similar distribution to that obtained from the linear MPR-32, and a pronounced double hump structure in the logarithmic part of the spectrum. The double hump structure (see Fig. 7) is related to the implantation of the ^{136}Xe ions. A detailed analysis of the implantation events showed that in most cases only one (88%) or two (11%) strips on the x- and y-side of DSSSD were activated, which is quite

different to the result with the linear MPR-32 (see Fig. 6, right). The highest energy peak could always be related to the implantation, while the second highest peak is due to the cross talk with the neighbouring strip. In 90% of all multiplicity two events the second highest peak was observed in the neighbouring strip. For the logarithmic MPR-32 preamplifier the mean of the highest peak of the double hump structure was used for the position determination. In summary, the measurement with the logarithmic preamplifier yields in 98% of all events an implantation within one strip, while the analysis with linear preamplifier determines, on average, a false shift of the implantation by 2.3 mm. Since no decay electrons were measured in this part of the study (^{136}Xe is a β -stable beam), a position correlation in x-direction between the DSSSD and a multi-wire (MW) detector of the FRS (in front of the active stopper) was determined. This is displayed in Fig. 8. It shows a strong correlation but also an offset since the DSSSD was not accurately centred in the frame of the FRS.

In conclusion, the logarithmic MPR-32 preamplifier is well suited for the active stopper of the RISING project. It covers a large energy range from fragment implantation down to β -decay. After the implantation of the exotic nuclei, the β -particles will be measured with high efficiency due to the low detection threshold of 150 keV. Since the DSSSDs are operated in dry nitrogen, a detector vessel with thin walls can be used to minimize the absorption of the emitted γ -rays. The excellent energy resolution of 20 keV also allows conversion electron spectroscopy to be performed as part of the stopped beam RISING campaign. Such an electron conversion measurement on ^{205}Au [10] was successfully performed with the present setup.

Acknowledgements

This work is supported by EPSRC (UK) and EURONS (EU Contract number 506065). Work partially supported by Spanish MEC, Grants FPA2005-03993 and FPA2005-00732. A.A. recognizes partial support of the Ramon y Cajal program.

References

- [1] S. Pietri, et al., Nucl. Instr. and Meth. B 261 (2007) 1079.
- [2] Micron Semiconductor Ltd., Marlborough Road, Lancing Sussex, England (www.micronsemiconductor.co.uk).
- [3] S. Agostinelli, et al., Nucl. Instr. and Meth. A 506 (2003) 250.
- [4] S. Chauvie, et al., in: Nuclear Science Symposium Conference Record, vol. 3, IEEE, New York, 2004, p. 1881.
- [5] H. Geissel, et al., Nucl. Instr. and Meth. B 70 (1992) 286.
- [6] Mesytec GmbH, Werner Von Braun Str. 1, D-85640 Putzbrunn, Germany (www.mesytec.com).
- [7] Multi Channel Systems, Aspenhastrasse 21, D-72770 Rutlingen, Germany (www.multichannelsystems.com).
- [8] J.I. Prisciandaro, et al., Nucl. Instr. and Meth. A 505 (2003) 140.
- [9] J. Elson, Pico Systems, 543 Lindeman Rd., Kirkwood, MO (elson@pico-systems.com) (pico-systems.com/shapdisc.html).
- [10] Zs. Podolyak, et al., in: Proceedings of the International Symposium on Physics of Unstable Nuclei (ISPUN07), World Scientific, Singapore, 2008, pp. 48–55 and Phys. Lett. B, submitted for publication.

Enhanced strength of the $2_1^+ \rightarrow 0_{g.s.}^+$ transition in ^{114}Sn studied via Coulomb excitation in inverse kinematics

P. Doornenbal,^{1,2,*} P. Reiter,¹ H. Grawe,² H. J. Wollersheim,² P. Bednarczyk,^{2,3} L. Caceres,^{2,4} J. Cederkäll,^{5,6} A. Ekström,⁶ J. Gerl,² M. Górska,² A. Jhingan,⁷ I. Kojouharov,² R. Kumar,⁷ W. Prokopowicz,² H. Schaffner,² and R. P. Singh⁷

¹*Institut für Kernphysik, Universität zu Köln, D-50937 Köln, Germany*

²*Gesellschaft für Schwerionenforschung mbH, D-64291 Darmstadt, Germany*

³*The Niewodniczanski Institute of Nuclear Physics, Polish Academy of Sciences, 31-342 Krakow, Poland*

⁴*Departamento de Física Teórica, Universidad Autónoma de Madrid, E-28049 Madrid, Spain*

⁵*PH Department, CERN, 1211 Geneva, Switzerland*

⁶*Department of Physics, Lund University, 22100 Lund, Sweden*

⁷*Inter-University Accelerator Centre, New Delhi 110 067, India*

(Received 18 July 2008; published 22 September 2008)

The 2_1^+ states of $^{114,116}\text{Sn}$ were excited in two consecutive experiments by means of Coulomb excitation in inverse kinematics on a ^{58}Ni target. A precise determination of the reduced transition probability $B(E2; 0_{g.s.}^+ \rightarrow 2_1^+)$ of ^{114}Sn relative to the well-known 2_1^+ excitation strength in ^{116}Sn was achieved by comparing the relative projectile to target $2_1^+ \rightarrow 0_{g.s.}^+$ decay intensities. The obtained $B(E2 \uparrow)$ value of $0.232(8) e^2 b^2$ for ^{114}Sn confirms the tendency of large $B(E2 \uparrow)$ values for the light tin isotopes below the midshell ^{116}Sn that has been observed recently in various radioactive ion beam experiments. The result establishes most clearly the discrepancy between the current $B(E2 \uparrow)$ value predictions from large-scale shell-model calculations and the experimental deviation, which commences already for the stable ^{114}Sn isotope.

DOI: 10.1103/PhysRevC.78.031303

PACS number(s): 23.20.Js, 25.70.De, 27.60.+j

The ongoing development of new research facilities for experiments with unstable exotic nuclei has enabled nuclear structure investigations far away from the line of β stability. Most especially, the structure around ^{100}Sn has been spotlighted recently by experimental and theoretical research, as it is presumably the heaviest, particle bound, doubly magic $N = Z$ nucleus. In this context, the systematic study of nuclear properties along the semi magic, $Z = 50$ tin isotopes is of grand interest because the evolution of the proton gap can be experimentally probed in between two major shell closures.

The excitation energies from the ground state (g.s.) to the 2_1^+ state between ^{102}Sn and ^{130}Sn are well established and possess an almost constant value [1], which is expected for semimagic nuclei in the generalized seniority scheme (see, e.g., Ref. [2]). A sensitive probe for the robustness of the $Z = 50$ shell closure along the chain of even tin isotopes between the two neutron shell closures at $N = 50$ and $N = 82$ is provided by the reduced transition probability, the $B(E2; 0_{g.s.}^+ \rightarrow 2_1^+)$ value, henceforth abbreviated as $B(E2 \uparrow)$. The $E2$ transition strengths in stable even tin isotopes ($^{112-124}\text{Sn}$) are accurately known except for that of ^{114}Sn . For this nucleus, the values obtained have been measured in two independent ways thus far with considerable errors that do not allow a firm conclusion on the evolution of the $B(E2 \uparrow)$ value at this isotope. The small natural abundance of the ^{114}Sn isotope of just 0.65% and the fact that ^{114}Sn and ^{116}Sn have almost identical 2_1^+ level energies of 1299.907(7) and 1293.560(8) keV [1], respectively, impedes the direct approach via Coulomb excitation on a natural tin target. In two experiments with enriched ^{114}Sn targets values

of $0.20(7) e^2 b^2$ and $0.25(5) e^2 b^2$ were obtained [3,4]. More recently, Doppler-shift attenuation lifetime measurements were performed and values of $0.27(9) e^2 b^2$ and $0.19(4) e^2 b^2$ were deduced [5,6]. All these results lead to an accepted value of $0.24(5) e^2 b^2$ [1] with a considerable experimental uncertainty.

For unstable nuclei, lifetime measurements from, e.g., fusion-evaporation reactions are hindered by higher-lying isomeric states in the ns range. The $B(E2 \uparrow)$ values are thus accessible preferentially via Coulomb excitation from the ground state employing radioactive beam techniques. On the neutron-rich side, this has been achieved recently [7]. For the proton-rich side, several Coulomb excitation experiments have been performed at relativistic, intermediate, and sub-barrier energies for the nuclei $^{106,108,110}\text{Sn}$ [8–11]. The derived $B(E2 \uparrow)$ values from these experiments are plotted in Fig. 1 together with the excitation strengths of stable tin nuclei evaluated in Ref. [1]. Two different trends are observed for the chain of tin nuclei: while at the neutron-rich side drop considerably with increasing neutron number, an almost constant plateau of high $B(E2 \uparrow)$ values emerges on the proton-rich side.

These unexpectedly high $B(E2 \uparrow)$ values caused a persistent discrepancy between the results of new large-scale shell model (LSSM) calculations [8] and experimental findings. The LSSM calculation, using a polarization charge of $0.5e$ for protons and neutrons, has been performed with admixtures of up to $4p4h$ proton excitations across the $Z = 50$ shell gap to enhance the transition strength considerably over a pure neutron valence space calculation with a closed $Z = 50$ core [8,10]. In the latter approach the enhancement is achieved by introducing an effective neutron charge of $1.0e$. Both calculations, however, yield a parabolically shaped systematics of the $B(E2 \uparrow)$ with mass number A and fail to reproduce the

*Present address: RIKEN Nishina Center for Accelerator-Based Science, Wako, Saitama 351-0198, Japan.

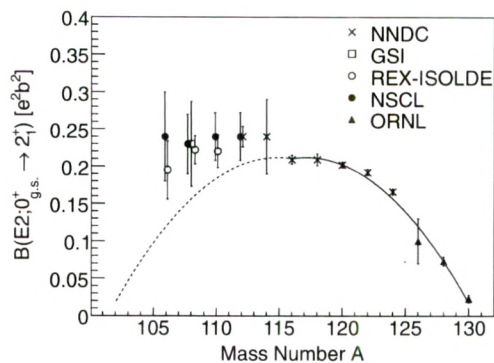


FIG. 1. Experimental $B(E2 \uparrow)$ values in even-even tin isotopes. Data are taken from Refs. [1,7–11]. The statistical and systematic uncertainties of Ref. [9] were added quadratically. A parabolic fit has been applied to the nuclei ranging from $A = 116$ –130 (solid line), which has been mirrored around $A = 116$ for the proton-rich side (dashed line).

asymmetric trend of the experimental results. This is clearly demonstrated by the symmetric lower shell continuation (dashed line) of the parabola fitted to the $A = 116$ –130 values (full line) to guide the eye.

The inaccurate $B(E2 \uparrow)$ value of ^{114}Sn motivated a Coulomb excitation experiment with a stable beam in inverse kinematics to improve this crucial data point and to firmly establish the location along the Sn isotope chain where the $B(E2 \uparrow)$ value is increased. Because a stable tin beam does not suffer from low beam intensities, the $E2$ excitation strength can be determined with a high accuracy from a γ -ray measurement. Two stable tin nuclei seem to belong to the region of enhanced $B(E2 \uparrow)$ values: ^{112}Sn and ^{114}Sn . For the former nucleus previous Coulomb excitation results [3,4,12,13] have been confirmed recently by means of lifetime measurements employing the Doppler-shift attenuation method [14]. For ^{114}Sn , the large experimental error prohibits definite conclusions about the exact $B(E2 \uparrow)$ evolution. Therefore, we performed two consecutive Coulomb excitation experiments using ^{114}Sn and ^{116}Sn beams with “safe” beam energies well below the Coulomb barrier to determine the relative excitation strengths between both tin isotopes in inverse kinematics on the same target. In this way systematic errors can be excluded and the target excitation cancels for the $^{114}\text{Sn}/^{116}\text{Sn}$ γ -ray yield ratio. These γ -ray yield data are a direct measure of the $B(E2 \uparrow)$ ratio of ^{114}Sn relative to ^{116}Sn . Note that the adopted $B(E2 \uparrow)$ value for ^{116}Sn of $0.209(6) e^2 b^2$ is an evaluation of fifteen different experimental results [1] and is, therefore, a reliable and precise reference point.

The tin beams were provided by the UNILAC accelerator at Gesellschaft für Schwerionenforschung (GSI) with an energy of $3.4A$ MeV. Beam particles were incident on a 0.7-mg/cm^2 ^{58}Ni target with a purity of 99.9%. An annular gas-filled parallel plate avalanche counter (PPAC) was placed 13 cm downstream of the target to detect both the scattered projectiles as well as the recoiling target nuclei. The PPAC consisted of an anode foil, subdivided into 20 radial segments for the azimuthal angle φ_{lab} information, and a cathode plate of 50 concentric rings connected by an electronic

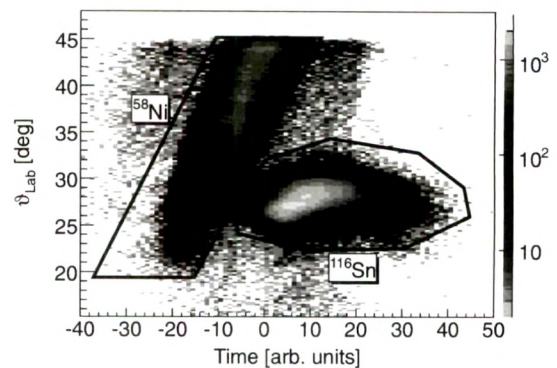


FIG. 2. Scattered projectile and target nuclei coincidences were detected in the PPAC for the ^{116}Sn beam incident on the ^{58}Ni target. The scattering angle is plotted versus the time of flight differences of both reaction partners. The corresponding kinematical cuts applied for coincident γ rays are indicated. See text for details.

delay line with 2-ns time delay steps. The polar angle ϑ_{lab} was deduced by measuring the delay line time differences between signals coming from the innermost and outermost ring. The PPAC covered an angular range of $15^\circ \leq \vartheta_{\text{lab}} \leq 45^\circ$. Because the PPAC was split into two independent parts, kinematical coincidences between projectiles and ejectiles were measured within this angular range. For ejectiles detected in the PPAC, the corresponding scattering angles of ^{114}Sn and ^{116}Sn varied between $24^\circ \leq \vartheta_{\text{lab}} \leq 31^\circ$. To identify projectile and target nucleus, the time of flight differences between both scattered particles was measured. Figure 2 shows the measured scattering angle of one detector half as a function of the time difference. The figure presents data from the ^{116}Sn beam striking on the ^{58}Ni target as an example. It demonstrates the unambiguous assignments of the measured scattering angles in both PPAC halves to projectile and target nucleus, respectively.

De-excitation γ rays emitted after Coulomb excitation were measured with two Superclover (Ge) detectors mounted at an angle of $\vartheta_\gamma = 25^\circ$ relative to the beam axis in the forward direction at a distance of 20 cm from the target. Each detector consisted of four coaxial N-type Ge crystals, arranged like a four leaf clover. The two detectors had a total photopeak efficiency of $\approx 1\%$ and an energy resolution of 3.8 keV [full width at half maximum (FWHM)] at 1332.5 keV. To suppress low energetic radiation, the front sides of the Superclover detectors were covered by a stacked shielding of 0.2-mm Ta, 1.0-mm Sn, and 0.5-mm Cu plates. Scattered particles hitting the PPAC had velocities of up to $\beta \approx 10\%$ for the target nuclei, whereas the projectiles retained velocities of up to $\beta \approx 6\%$. A Doppler correction was applied only when both reaction particles and at least one γ ray were detected. Although the lower angular coverage of the PPAC was $\vartheta_{\text{lab}} = 15^\circ$, two-particle events were detected only for target nucleus angles above $\vartheta_{\text{lab}} \approx 20^\circ$. This restriction was caused by the low projectile residual energy for a high center-of-mass $\vartheta_{\text{c.m.}}$ scattering angle and pertained to ^{114}Sn and ^{116}Sn in equal measure. Due to the PPAC polar angle resolution of 2° , the scattering angle of the projectile and, accordingly, the velocity were best determined by a reconstruction from the position information

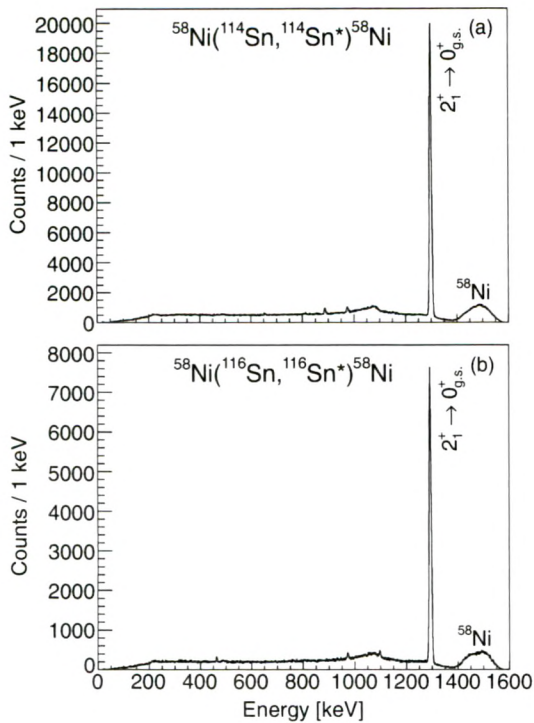


FIG. 3. Doppler corrected γ -ray spectra associated with a coincidence of two particles in the PPAC. The Doppler correction was applied using the kinematical information of the target nuclei but assuming a projectile excitation of ^{114}Sn (a) and ^{116}Sn (b), respectively. The elevation between 1400 and 1600 keV corresponds to decays from the 2_1^+ state of the ^{58}Ni ejectiles.

of the target nucleus and hence used for the Doppler correction. A γ -ray energy resolution of 0.7% (FWHM) was obtained for decays from projectile excitation and 1.0% (FWHM) for decays from target excitation. The difference was caused by the Doppler broadening due to the higher velocity of the latter particles. Figure 3 shows the Doppler-corrected spectra for projectile excitation of ^{114}Sn and ^{116}Sn . Clearly, the spectra are dominated by the $2_1^+ \rightarrow 0_{g.s.}^+$ transitions. Higher excited states were only weakly populated. Namely transitions from the 0_2^+ , 3_1^- , 4_1^+ states to the respective 2_1^+ state were detected with much lower intensity. In both cases the summed intensity from decays of higher-lying states added up to less than 4% of the $2_1^+ \rightarrow 0_{g.s.}^+$ decay intensity.

To obtain the $B(E2 \uparrow)$ value in ^{114}Sn , the experimental γ -ray intensity double ratio $I_\gamma(^{114}\text{Sn})/I_\gamma(^{58}\text{Ni})/I_\gamma(^{116}\text{Sn})/I_\gamma(^{58}\text{Ni})$ of the $2_1^+ \rightarrow 0_{g.s.}^+$ decays was determined. The observed feeding was subtracted from the 2_1^+ intensities. The experimental double ratio was compared with Coulomb excitation calculations from the Winther-de Boer COULEX code [15]. The calculations included the feeding contributions from the 0_2^+ , 3_1^- , 4_1^+ states in ^{114}Sn and ^{116}Sn , which were obtained from the known excitation strengths given in Ref. [1]. The $0_{g.s.}^+ \rightarrow 2_1^+$ matrix element in ^{114}Sn was adjusted in the COULEX calculations to reproduce the experimental double ratio. As a result, the $B(E2 \uparrow)$ value in ^{114}Sn was determined as $0.232(8) e^2 b^2$. The error is the quadratic sum of the individual

uncertainties of the γ -ray intensities (1%), the adopted ^{116}Sn $B(E2 \uparrow)$ value (3%), and the angular range acceptance of the PPAC (1%). The latter error accounted for slightly different particle detection efficiencies in ^{114}Sn and ^{116}Sn at high center-of-mass scattering angles and, accordingly, low projectile energies; and for different beam spots on the target in the two experiments (≈ 3 -mm deviation). It is noteworthy that the double ratio has a negligible dependence ($\ll 1\%$) on the selected scattering angle range if both ranges are identical and the singles ratios $I_\gamma(^{114,116}\text{Sn})/I_\gamma(^{58}\text{Ni})$ vary only slightly by less than 10% from the lowest accepted scattering angle ($\vartheta_{c.m.} = 90^\circ$) to the highest ($\vartheta_{c.m.} = 140^\circ$), respectively. In summary, the new $B(E2 \uparrow)$ value of $0.232(8) e^2 b^2$ for the first excited 2^+ state in ^{114}Sn is a significant improvement with respect to the previous insufficient situation. Moreover, the new result is also, with its reduced error limits, clearly consistent with all previous values.

Our deduced $B(E2 \uparrow)$ value of ^{114}Sn is included in the experimental $B(E2 \uparrow)$ systematics of Fig. 4 and shows, with the smallest uncertainty, an increased $B(E2 \uparrow)$ value with respect to the neighboring midshell nuclei. Thus, our result demonstrates that the experimental asymmetry toward an enhanced $E2$ transition strengths commences with ^{114}Sn as the anchor point for the deviating trend.

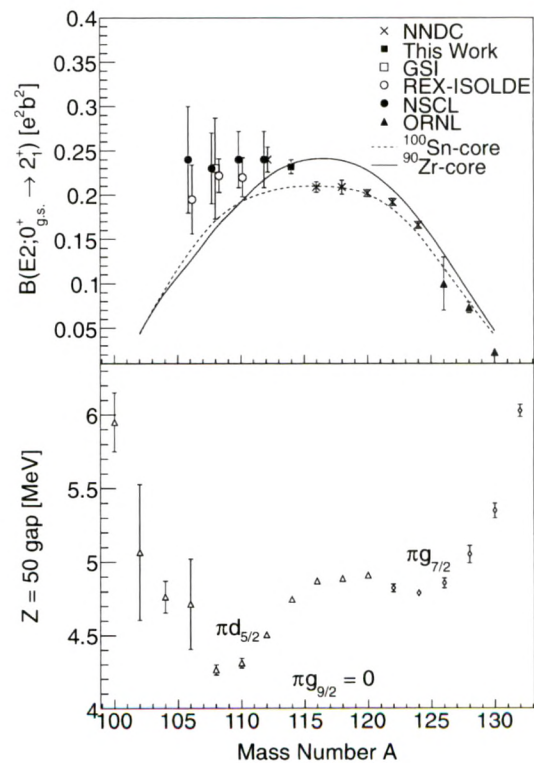


FIG. 4. The upper panel displays a comparison of the new experimental $B(E2 \uparrow)$ value from the present work and data from Refs. [1,7,8,10,11] for even-even tin isotopes with LSSM calculations presented in Ref. [8] using a ^{100}Sn (dotted line) and ^{90}Zr (solid line) closed-shell core, respectively. The lower panel shows the experimental $Z = 50$ gaps extracted from Refs. [18,19].

Within the work on ^{108}Sn by Banu and collaborators [8], the $B(E2 \uparrow)$ values for the $Z = 50$ tin isotopes have been determined theoretically by means of state-of-the-art large-scale shell-model calculations. These calculations used an effective interaction derived with the G -matrix prescription [16] from the CD-Bonn nucleon-nucleon potential [17] with the two different closed shell cores of ^{90}Zr ($\text{SM}_{\pi\nu}$) and ^{100}Sn (SM_ν), respectively. $\text{SM}_{\pi\nu}$ uses a proton $\pi(g, d, s)$ and neutron $\nu(g_{7/2}, d_{5/2}, s_{1/2}, h_{11/2})$ model space. Up to $4p4h$ excitations were allowed across the $Z = 50$ closed shell and $B(E2 \uparrow)$ values were calculated with a common polarization charge of $0.5e$ for protons and neutrons. For SM_ν a pure neutron $\nu(g_{7/2}, d_{5/2}, s_{1/2}, h_{11/2})$ model space and an effective neutron charge of $1.0e$ were employed to account for the neglect of proton core excitations. For both cases, the theoretical curve is parabolic and symmetric with respect to the midshell nucleus ^{116}Sn , as shown in Fig. 4, causing the puzzling discrepancies between experiment and theory for the lighter tin isotopes. The $\text{SM}_{\pi\nu}$ calculation agrees with the new experimental $^{114}\text{Sn} B(E2 \uparrow)$ of the present work, but overpredicts the $A \geq 116$ values, whereas the lower-shell values seem to be underestimated despite of the large experimental uncertainties. Similarly, the SM_ν approach agrees with the upper-shell values but underpredicts the $E2$ strengths in the light Sn isotopes.

Since the LSSM calculations presented with the first radioactive beam experiment on ^{108}Sn [8], recent experiments on $^{106-110}\text{Sn}$ [9–11] confirmed the deviation from a symmetric behavior of the $B(E2 \uparrow)$. Several qualitative arguments for future improvements of shell-model calculations, such as excitations across the $N = 50$ shell [8], α correlations due to proton $2p2h$ excitations [9], refined tuning of proton-neutron monopoles [8,10], or even a reduction of the $Z = N = 50$ shell gaps [11] have been brought forward. In the lower panel of Fig. 4 the experimental $Z = 50$ shell gaps are shown for $N = 50-82$ [18]. The ^{100}Sn value was extrapolated from experimental proton $g_{9/2}$ and $d_{5/2}$ single-particle energies in ^{90}Zr by using empirical two-body matrix elements including Coulomb repulsion [19]. From ^{132}Sn , the well-known reduction of the proton gap toward the neutron midshell is observed, which is due to proton-neutron induced cross-shell excitations. The gap stays constant between $N = 76$ and 66 with the $\pi g_{7/2}$ and $\pi d_{5/2}$ crossing at $N = 70$. Below $N = 66$ ($A = 116$) the gap reduces gradually by about 600 keV before it increases toward the double shell closure at $N = 50$. This is exactly the region where the $B(E2 \uparrow)$ values deviate from symmetry and the shell-model trend. It is known from LSSM calculations [8] that the major contribution to the $B(E2 \uparrow)$ stems from proton

excitations across $Z = 50$, as can be inferred from the $t = 0$ and $t = 4$ curves in Fig. 3 of Ref. [8]. Moreover, these excitations are dominated by the large stretched $\pi g_{9/2} \rightarrow \pi d_{5/2}$ $E2$ matrix element. In terms of monopole driven shell evolution [20–23], the reduction of the shell gap can be clearly attributed to the emptying of the neutron $\nu g_{7/2}$ orbit below $N = 66$. This will lift the $\pi g_{9/2}$ relative to the $\pi d_{5/2}$ and hence reduce the gap, which is decisive for $E2$ core polarization. The respective monopoles $V^m(\pi g_{9/2} \nu j)$ are largely different for the $g_{9/2}$ spin flip partner $j = g_{7/2}$ and $j = d_{5/2}$ [20,22–24]. This causes the experimentally well-established dramatic decrease of the $\nu g_{7/2} - \nu d_{5/2}$ distance in $N = 51$ isotones on filling of the $\pi g_{9/2}$ orbit between ^{91}Zr and ^{101}Sn (see, e.g., Ref. [24]) and acts in a similar way on the $\pi g_{9/2}$ orbit when filling (respective emptying) the $\nu g_{7/2}$ shell along the $Z = 50$ isotopic chain. The decrease is less pronounced due to the near degeneracy of the neutron $g_{7/2}$ and $d_{5/2}$ orbits leading to a simultaneous filling (emptying) of the two and to the effect of the smaller $\nu g_{7/2} - \pi d_{5/2}$ monopole $V^m(\pi d_{5/2} \nu g_{7/2})$. It is therefore concluded that (i) proton excitations across a reduced $Z = 50$ gap are responsible for the enhanced $B(E2 \uparrow)$ values below $A = 116$ and that (ii) interactions used in LSSM calculations need monopole tuning to reproduce both the evolution of the experimental $Z = 50$ gap and the $B(E2 \uparrow)$. It should be noted that the described scenario implies that in $^{102,104}\text{Sn}$ the $B(E2 \uparrow)$ values will return to be normal. For ^{100}Sn , the empirical shell gap extrapolation results in a reduction of the proton gap of about 800 keV relative to the neutron gap [19].

In summary, we have determined the $B(E2 \uparrow)$ value in ^{114}Sn relative to the well-known value of ^{116}Sn with a high accuracy. The deduced excitation strength of $0.232(8)e^2b^2$ marks the key starting point for the striking deviation from a symmetric trend around the $N = 66$ neutron midshell that was observed from radioactive beam experiments in the proton-rich $^{106-110}\text{Sn}$. This implies a disagreement with current large-scale shell-model calculations and suggests the need for a refined tuning of the two-body interactions employed. Further experimental studies as well as theoretical investigations of the $Z = 50$ and $N = 50$ gaps are of substantial importance to enlighten the nuclear structure in the vicinity of the doubly magic ^{100}Sn .

The authors thank the GSI accelerator staff for providing the tin beams and appreciate shell-model discussions with F. Nowacki. One author (P.D.) is grateful for the support by the JSPS.

-
- [1] S. Raman, C. W. Nestor, and P. Tikkanen, *At. Data Nucl. Data Tables* **78**, 1 (2001).
 [2] R. Casten, *Nuclear Structure from a Simple Perspective* (Oxford University Press, New York, 2000).
 [3] D. G. Alkhazov, D. S. Andreev, K. I. Erokhina, and I. K. Lemberg, *Zh. Eksp. Teor. Fiz.* **33**, 1347 (1957) [*Sov. Phys. JETP* **6**, 1036 (1958)].
 [4] D. S. Andreev, V. D. Vasilev, G. M. Gusinskii, K. I. Erokhina, and I. K. Lemberg, *Izv. Akad. Nauk SSSR, Ser. Fiz.* **25**, 832 (1961); *Columbia Tech. Transl.* **25**, 842 (1962).
 [5] I. N. Vishnevsky, M. F. Kudoyarov, E. V. Kuzmin, Yu. N. Lobach, A. A. Pasternak, and V. V. Trishin, in *Proceedings of the 41st Conference on Nuclear Spectroscopy and the Structure of the Atomic Nucleus*, Minsk (1991), p. 71.
 [6] J. Gableske *et al.*, *Nucl. Phys.* **A691**, 551 (2001).
 [7] D. C. Radford *et al.*, *Nucl. Phys.* **A752**, 264c (2005).
 [8] A. Banu *et al.*, *Phys. Rev. C* **72**, 061305(R) (2005).
 [9] C. Vaman *et al.*, *Phys. Rev. Lett.* **99**, 162501 (2007).
 [10] J. Cederkäll *et al.*, *Phys. Rev. Lett.* **98**, 172501 (2007).

- [11] A. Ekström *et al.*, Phys. Rev. Lett. **101**, 012502 (2008).
- [12] P. H. Stelson, F. K. McGowan, R. L. Robinson, and W. T. Milner, Phys. Rev. C **2**, 2015 (1970).
- [13] R. Graetzer, S. M. Cohick, and J. X. Saladin, Phys. Rev. C **12**, 1462 (1975).
- [14] J. N. Orce, S. N. Choudry, B. Crider, E. Elhami, S. Mukhopadhyay, M. Scheck, M. T. McEllistrem, and S. W. Yates, Phys. Rev. C **76**, 021302(R) (2007); Phys. Rev. C **77**, 029902(E) (2008).
- [15] A. Winther and J. De Boer, in *Coulomb Excitation*, edited by K. Alder and A. Winther (Academic Press, New York/London, 1966).
- [16] M. Hjorth-Jensen, T. T. S. Kuo, and E. Osnes, Phys. Rep. **261**, 125 (1995).
- [17] R. Machleidt, F. Sammarruca, and Y. Song, Phys. Rev. C **53**, R1483 (1996).
- [18] A. H. Wapstra, G. Audi, and C. Thibault, Nucl. Phys. A **729**, 337 (2003).
- [19] H. Grawe, K. Langanke, and G. Martínez-Pinedo, Rep. Prog. Phys. **70**, 1525 (2007).
- [20] T. Otsuka, R. Fujimoto, Y. Utsuno, B. A. Brown, M. Honma, and T. Mizusaki, Phys. Rev. Lett. **87**, 082502 (2001).
- [21] H. Grawe, Acta Phys. Pol. B **34**, 2267 (2003).
- [22] H. Grawe, *Lecture Notes in Physics* (Springer, Berlin/Heidelberg, 2004), Vol. 651, p. 33.
- [23] T. Otsuka, T. Suzuki, R. Fujimoto, H. Grawe, and Y. Akaishi, Phys. Rev. Lett. **95**, 232502 (2005).
- [24] H. Grawe, A. Blazhev, M. Gorska, R. Grzywacz, H. Mach, and I. Mukha, Eur. Phys. J. A **27**, s01, 257 (2006).